

# Iterative feedback control based on frequency response model for a six-degree-of-freedom micro-vibration platform

He Zhu<sup>1,2</sup> , Shuai He<sup>2,3</sup>, Zhenbang Xu<sup>2,3</sup>, XiaoMing Wang<sup>2,3</sup>, Chao Qin<sup>2,3</sup>, Jianfeng Yang<sup>4</sup> and Lei Zhang<sup>1,5</sup>

Journal of Vibration and Control  
2022, Vol. 28(13-14) 1727–1738  
© The Author(s) 2021  
Article reuse guidelines:  
[sagepub.com/journals-permissions](https://sagepub.com/journals-permissions)  
DOI: 10.1177/1077546321997310  
[journals.sagepub.com/home/jvc](https://journals.sagepub.com/home/jvc)  


## Abstract

In this article, a six-degree-of-freedom (6-DOF) micro-vibration platform (6-MVP) based on the Gough–Stewart configuration is designed to reproduce the 6-DOF micro-vibration that occurs at the installation surfaces of sensitive space-based instruments such as large space optical loads and laser communications equipment. The platform's dynamic model is simplified because of the small displacement characteristics of micro-vibrations. By considering the multifrequency line spectrum characteristics of micro-vibrations and the parameter uncertainties, an iterative feedback control strategy based on a frequency response model is designed, and the effectiveness of the proposed control strategy is verified by performing integrated simulations. Finally, micro-vibration experiments are performed with a 10 kg load on the platform. The results of these micro-vibration experiments show that after several iterations, the amplitude control errors are less than 3% and the phase control errors are less than 1°. The control strategy presented in this article offers the advantages of a simple algorithm and high precision and it can also be used to control other similar micro-vibration platforms.

## Keywords

Micro-vibration platform, micro-vibration, frequency response, iterative control

## 1. Introduction

The micro-vibrations in space that are produced by a wide variety of the equipment on spacecraft, including refrigeration compressors, solar panel rotation mechanisms, and reaction flywheels, have a significant effect on pointing accuracy, stability, and other important performance indices for large-caliber, high-resolution optical loads (e.g., the James Webb Space Telescope and the Space Interferometry Mission). Vibration isolation is, therefore, necessary to reduce this disturbance effect. One particular type of vibration isolation application is reduction of the micro-vibrations that are transmitted to the mounting surface for an optical load. To test the isolation performance of isolators fully, six-degree-of-freedom (6-DOF) micro-vibration equipment is required for the ground experiments.

Because of the wide variety of possible disturbance sources and scheduling issues, it is unusual for all actual disturbances to be used (Kamesh et al., 2012; Liu et al., 2012; Zhou and Liu, 2013) to perform the ground experiments. Therefore, the development of a micro-vibration platform that can replace the actual disturbances would be a significant step in the development of high-resolution

optical loads. Park et al. (2012, 2014) proposed two different types of multidimensional micro-vibration simulator. One simulator consisted of six identical single-axis micro-vibration actuators configured in a “cube,” where only the

<sup>1</sup>University of Chinese Academy of Sciences, China

<sup>2</sup>Innovation Laboratory of Space Robot System, Space Robotics Engineering Center, Changchun Institute of Optics, Fine Mechanics and Physics, Chinese Academy of Sciences, China

<sup>3</sup>CAS Key Laboratory of On-Orbit Manufacturing and Integration for Space Optics System, Changchun Institute of Optics, Fine Mechanics and Physics, Chinese Academy of Sciences, China

<sup>4</sup>China Electronic Product Reliability and Environmental Testing Research Institute, China

<sup>5</sup>Changuang Satellite Technology Company, China

Received: 27 September 2020; accepted: 23 January 2021

### Corresponding authors:

Shuai He, Changchun Institute of Optics, Fine Mechanics and Physics, Chinese Academy of Sciences, Changchun 130033, Jilin, China.  
Email: [652740868@qq.com](mailto:652740868@qq.com)

Zhenbang Xu, Changchun Institute of Optics, Fine Mechanics and Physics, Chinese Academy of Sciences, Changchun 130033, Jilin, China.  
Email: [xuzhenbang@ciomp.ac.cn](mailto:xuzhenbang@ciomp.ac.cn)

single-axis actuator performances are tested. The second simulator generated multidimensional disturbances using three actuators that were mounted on three mutually perpendicular plate surfaces, but this emulator could only produce three disturbance forces. Lin (2019) improved a micro-vibration simulator to realize a six-dimensional force and moment output by determining the positional relationships of the six single-axis actuators and the equivalent force system on the basis of Park's proposed simulator. However, their simulator could not be used to generate acceleration.

Because of advantages that include high maneuverability, high precision, and high stiffness, the Gough–Stewart platform (GSP) has been used to reproduce micro-vibrations. Vose et al. (2013) designed a 6-DOF simulator that could produce a micro-vibration velocity field, but because of its flexible connecting pipes, the system bandwidth was not high enough. Wang et al. (2017) proposed a multi-degree-of-freedom micro-vibration simulator based on the GSP to reproduce the disturbance forces and moments generated in the 50–250 Hz frequency bandwidth range by the reaction/momentum wheel assembly.

However, modeling and control are the main topics of research on the GSP. Many researchers have established dynamic models of the GSP using various methods (Dasgupta and Mruthyunjaya, 1998; Oftadeh et al., 2010; Pedrammehr et al., 2012), but these dynamic models are very complex. In the GSP control field, several displacement feedback control methods (Guo et al., 2008; Kim et al., 2005; Yang et al., 2009) have been proposed. Yang et al. (2016) designed a robust proportional–integral controller for use in acceleration control of the micro-vibration parallel manipulator. Because of the small displacements involved in space micro-vibrations (in Toyoshima et al., 2010), the micro-vibration acceleration is approximately  $0.1\text{--}0.5\text{ m/s}^2$  and a displacement amplitude of approximately  $0.25\text{ }\mu\text{m}$  is required to obtain the  $0.1\text{ m/s}^2$  acceleration at 100 Hz, it is difficult to obtain displacement sensors with sufficiently high precision, and the displacement feedback control methods used are not suitable for control of the micro-vibration platform. To address this point, Wang et al. (2018) developed a closed-loop iterative control method based on a dynamic model to control a 6-DOF disturbance force and moment simulator within the frequency range from 50 to 120 Hz by multiplying an iterative coefficient matrix to approach the desired force and moment. However, this method was only suitable for control of variations in amplitude. The research presented in this article represents a further development based on Wang's research that not only controls the amplitude of the acceleration but also controls its phase.

In this article, a 6-DOF micro-vibration platform based on the Gough–Stewart configuration is introduced that can reproduce micro-vibrations with various amplitudes and frequencies. Because the complete dynamic equation for the proposed simulator is complex, the calculation speed is reduced and its control frequency bandwidth is affected. To enable faster calculations, the dynamic model in this study is

simplified because of the small displacement and angular velocity characteristics of the space micro-vibrations; in addition, to simplify the sensor layout requirements and gather the signals more easily, an iterative feedback control strategy based on the frequency response model is designed that considers the multifrequency line spectrum characteristics (2013) and parameter uncertainty of micro-vibrations, and the proposed control algorithm is verified via simulations. The micro-vibration platform then provides experimental micro-vibration test results when using the proposed control strategy. The experimental results verify that the control strategy can control the 6-DOF micro-vibration platform (6-MVP) to provide the desired micro-vibrations.

The remainder of this article is organized as follows. Section 2 introduces the 6-MVP structure. Section 3 simplifies the dynamic model of this platform. Section 4 proposes the iterative feedback control method for the acceleration and validates this control method through simulations. Section 5 presents the experimental measurement results for the six-dimensional acceleration characteristics that are produced by the simulator on a mounting surface. Finally, Section 6 draws conclusions about the performance of the 6-MVP.

## 2. Structure

The micro-vibration platform structure is shown in Figure 1(a). The 6-MVP consists of an upper platform, a lower platform, 30 hinges (including three upper hinges and two lower hinges in each leg), and six identical legs. Figure 1(b) shows the detailed structure of the leg, which is mainly composed of a voice coil motor, a cover, a spring piece, and a stopper. The voice coil motor is used to drive the leg. The cover provides support for both the motor and the spring piece and protects the internal components of the outrigger. The spring piece provides support for both the motor and the upper platform. The displacement-limited action of the stopper on the outrigger prevents the spring piece from being damaged as a result of excessive deformation. The 6-MVP is used to reproduce the 6-DOF micro-vibration that occurs at the installation surfaces of space-based sensitive instruments.

Figure 2 shows the working principle diagram of the 6-MVP. The system consists of a space micro-vibration simulator, a suspension system, the control system, and the experimental payload. The upper platform of the 6-MVP can achieve movement with 6-DOF by varying the length of its six legs. The control system can control the upper platform motion by controlling the driving leg motion of the simulator. In the ground experiments, the experimental payload is connected to the upper platform, and a suspension system is required to realize gravitational unloading of the experimental payload to ensure that the system can simulate the space environment accurately and also ensure the safety of the system.

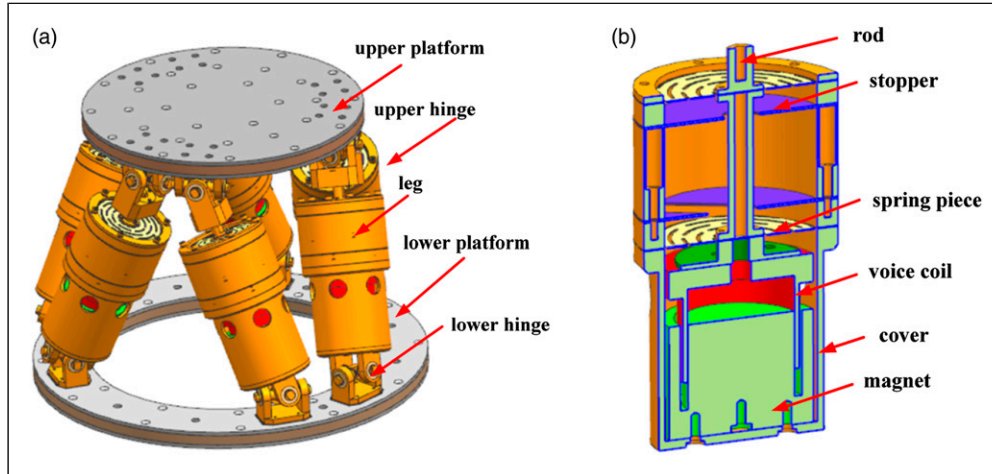


**Figure 1.** Structure of the micro-vibration platform: (a) micro-vibration platform structure and (b) detailed structure of the leg.

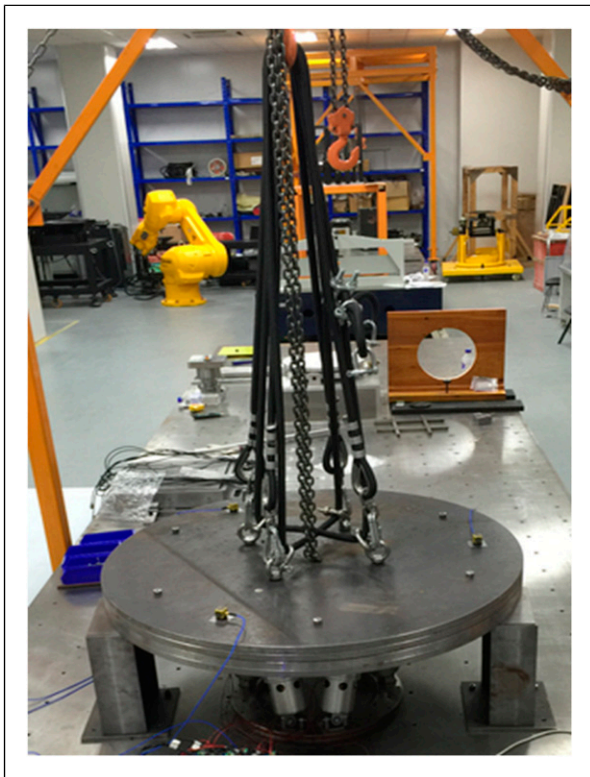


**Figure 2.** Working principle photograph of the six-micro-vibration platform.

### 3. Dynamic model

The scheme of the proposed vibration simulator is shown in Figure 3, in which the  $\{P\}$  coordinate system represents the body frame that is fixed to the geometric center of the joints of the moving platform, and the  $\{B\}$  coordinate system represents the base frame attached to the geometric center of the joints on the base plane. The  $\{g\}$  coordinate system

represents the inertial frame that is fixed to the geometric center at the bottom of the base plane, and its orientation is identical to that of frame  $\{B\}$ . The linear motions are described as surge ( $x$ ), sway ( $y$ ), and heave ( $z$ ) along the XB–YB–ZB axes of the base frame, and the angular motions of roll ( $\gamma$ ), pitch ( $\beta$ ), and yaw ( $\alpha$ ) are at X–Y–Z fixed angles. The upper joint points and the lower joint points are denoted by  $P_{pi}$  in frame  $\{P\}$  and  $B_{pi}$  in frame  $\{B\}$ , respectively.  $R_P$  and  $R_B$  denote the radii of the payload and the base platform, respectively. The angle between  $P_6$  and  $P_1$  is denoted by  $\varphi$ . The angle between  $B_6$  and  $B_1$  is denoted by  $\theta$ , as illustrated in Figure 3(b).

The complete dynamic equation for the vibration simulator was derived in an earlier article (Wang et al., 2017) and it is given by

$$M(q)\ddot{q} + C(q, \dot{q})\dot{q} + K \cdot \Delta q = J^T F \quad (1)$$

where  $J$  is the actuator Jacobian matrix that relates the general velocity of the platform to the actuator sliding velocities;  $M(q)$  is a  $6 \times 6$  mass matrix,  $C(q, \dot{q})$  is a  $6 \times 6$  matrix of the centrifugal and Coriolis force terms,  $K$  is a  $6 \times 6$  matrix of the generalized stiffness, and  $F$  is a  $6 \times 1$  vector that represents the actuator forces. The above matrices are given as follows

$$J = \begin{bmatrix} {}^B I_{n1}^T \cdot ({}^B_P R \cdot {}^P p_1 \times {}^B I_n^1)^T \\ {}^B I_{n2}^T \cdot ({}^B_P R \cdot {}^P p_2 \times {}^B I_n^2)^T \\ {}^B I_{n3}^T \cdot ({}^B_P R \cdot {}^P p_3 \times {}^B I_n^3)^T \\ {}^B I_{n4}^T \cdot ({}^B_P R \cdot {}^P p_4 \times {}^B I_n^4)^T \\ {}^B I_{n5}^T \cdot ({}^B_P R \cdot {}^P p_5 \times {}^B I_n^5)^T \\ {}^B I_{n6}^T \cdot ({}^B_P R \cdot {}^P p_6 \times {}^B I_n^6)^T \end{bmatrix} \quad (2)$$

where  ${}^B I_{ni}$  is the unit vector of the length vector  ${}^B I_i$  of the leg with respect to the base frame  $\{B\}$ , and  ${}^B_P R$  is the rotation

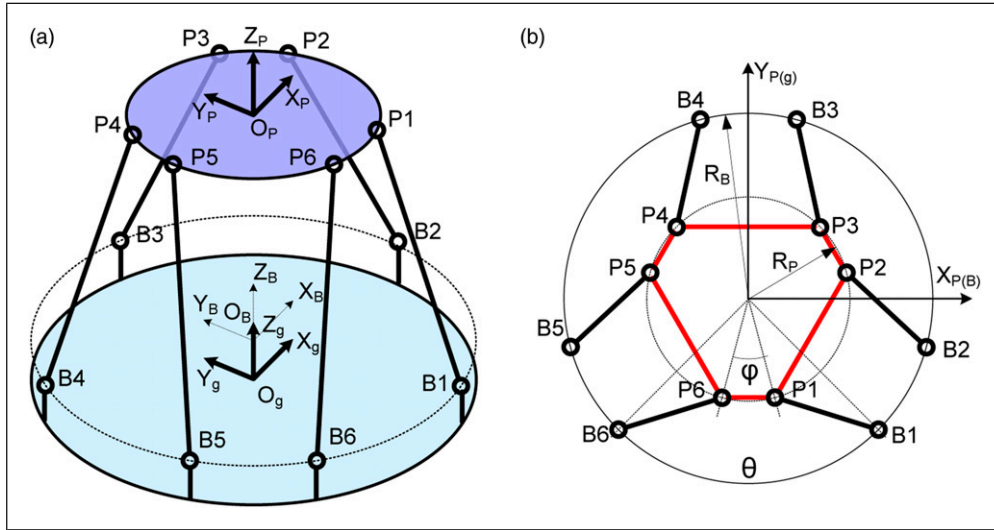


**Figure 3.** Schematic views of the vibration simulator: (a) Isometric view and (b) vertical view.

matrix of the transformation from the moving frame  $\{P\}$  to the base frame  $\{B\}$

$$M(q) = \begin{bmatrix} mE_3 & m \cdot {}^B R \cdot {}^P \tilde{p}_c^T \cdot {}^B R^T \\ m \cdot {}^B R \cdot {}^P \tilde{p}_c \cdot {}^B R^T & {}^B R \cdot {}^P I \cdot {}^B R^T \end{bmatrix} + \sum_{i=1}^6 {}^{pi} J_q^T M_{leg}^i {}^{pi} J_q \quad (3)$$

where  $E_3$  is a unit  $3 \times 3$  matrix,  $m$  is the payload mass,  ${}^{pi} J_q = [E_3, {}^B R \cdot {}^P \tilde{p}_c^T \cdot {}^B R^T]$  is the Jacobian matrix that relates the general velocity to the velocity of the upper joint  $P_i$ ,  ${}^P I$  is the inertia matrix with respect to frame  $\{P\}$ , and  ${}^P \tilde{p}_c$  is the skew symmetry matrix of  ${}^P p_c$

$$C(q, \dot{q}) \dot{q} = \left( \begin{bmatrix} 0 & 0 \\ 0 & \tilde{\omega}^B R \cdot {}^P I \cdot {}^B R^T \end{bmatrix} + c \cdot J^T J \right) \dot{q} + \sum_{i=1}^6 ({}^{pi} J_i^T) C_a^i {}^{pi} J_i \dot{q} + \begin{bmatrix} mE_3 \\ \mathbf{0} \end{bmatrix} \tilde{\omega}^2 ({}^B R \cdot {}^P p_c) + \sum_{i=1}^6 {}^{pi} J_{iT} M_{leg}^i \tilde{\omega}^2 ({}^B R \cdot {}^P p_i) \quad (4)$$

where  ${}^P I$  is the inertia matrix with respect to frame  $\{P\}$ ,  $\dot{q}$  is the general velocity of the moving platform,  $M_{leg}^i = {}^{rci} J_{pi}^T m_{rci} + {}^{tci} J_{pi}^T m_{tci} + \tilde{I}_{ni}^{T B} \tilde{I}_{ni} (I_r^i + I_t^i) / l_i^2$ , and  ${}^{rci} J_{pi}$  and  ${}^{tci} J_{pi}$  denote the Jacobian matrices relating the velocity of the upper joint  $P_i$  to the velocities of the upper leg and the lower leg centroid, respectively.  $\tilde{I}_{ni}$  represents the moments of inertia of the leg with respect to frame  $\{B\}$ , and  $I_r^i$  and  $I_t^i$  represent the principal moments of inertia of the upper leg and the lower leg, respectively

$$K = k \cdot J^T \cdot J \quad (5)$$

where  $k$  is the axial stiffness coefficient.

Because the displacement and the angular velocity of each micro-vibration is very small,  $J$ ,  $K$ , and  $M(q)$  can be treated as a constant matrix that is equal to the matrix at the initial equilibrium ( $q = [0, 0, 0, 0, 0, 0]^T$ ). At the same time, the square term of the angular velocity can be ignored and equation (4) can be reduced to

$$C(q, \dot{q}) \dot{q} = c \cdot J^T J \dot{q} \quad (6)$$

where  $c$  is the damping coefficient.

## 4. Control strategy and simulation

The uncertainty over the parameter values (e.g., the payload mass, the inertial tensor, and the stiffness of the springs) means that an actual micro-vibration platform will not coincide exactly with the theoretical model and a control strategy, therefore, must be implemented. Because the simulation platform is only required to reproduce the vibration of a multifrequency line spectrum, which is the main form of micro-vibration (Zhou et al., 2012), and trajectory tracking does not need to be achieved, the control method required can then be simplified. The vibration of the multifrequency line spectrum is a steady-state process and can be controlled using the frequency response function, which is obtained via the derivation below.

### 4.1. Frequency response analysis

By performing a Laplace transform on both sides of equation (1) and setting the initial condition to zero, the equation is then changed to

$$(Ms^2 + Cs + K)q(s) = J^T F(s) \quad (7)$$

By setting  $s = j\omega$  and multiplying both sides by  $(J^T)^{-1}$ , the frequency response function of the system is

$$F(j\omega) = (J^T)^{-1}(-M\omega^2 + jC\omega + K)q(j\omega) \quad (8)$$

The acceleration is the second derivative of the displacement, and the relationship between the acceleration  $A(j\omega)$  and the displacement  $q(j\omega)$  in the frequency domain is

$$A(j\omega) = -\omega^2 q(j\omega) \quad (9)$$

Substitution of equation (9) into (8) produces the following relationship between the accelerations and the motivating forces.

$$F(j\omega) = H(\omega)A(j\omega) \quad (10)$$

Here,  $H(\omega)$  is the frequency response function of the motivating forces relative to the upper platform accelerations, which can be written as

$$H(\omega) = -\frac{(J^T)^{-1}(-M\omega^2 + jC\omega + K)}{\omega^2} \quad (11)$$

## 4.2. Control strategy

The initial forces are obtained from  $F_0(\omega_i) = H(\omega_i)A(\omega_i)$ . Let  $F_j(\omega_i)$  be the control forces at step  $j$ , let  $A_j(\omega_i)$  be the actual output accelerations at step  $j$ , let  $A(\omega_i)$  be the desired accelerations, and let  $e_j(\omega_i) = A_j(\omega_i) - A(\omega_i)$  be the deviation of the actual output accelerations from the desired accelerations. The control input forces for step  $j + 1$  are then updated using an iterative control penalty as follows

$$F_{j+1}(\omega_i) = F_j(\omega_i) - K_j(\omega_i)H(\omega_i)e_j(\omega_i) \quad (12)$$

where  $K_j(\omega_i)$  is the controller gain at a frequency  $\omega_i$ . In this study,  $K_j(\omega_i)$  was set at 1.0 to achieve the desired control effect. Figure 4 shows an iterative flowchart for this procedure.

## 4.3. Simulation

Co-simulations using ADAMS and MATLAB/Simulink software are performed to verify the validity of both the simplified dynamic model and the control method. ADAMS is used to build a virtual prototype of the 6-MVP and output the accelerations of the upper platform, whereas MATLAB/Simulink uses the control model to compute the actuator forces.

The validity of the simplified dynamic model is verified by comparing the target response with the actual response to the initial control force when the control model's parameters are consistent with the virtual prototype's parameters. Tables 1 and 2 show the parameters of the virtual prototype.

The upper platform is allowed to reproduce three translational acceleration trajectories and three angular acceleration trajectories simultaneously, that is

$$\begin{aligned} A_x &= 0.01 \sin(2\pi \times 50t + 10 \times \pi/180) \\ &\quad + 0.06 \sin(2\pi \times 80t + 30 \times \pi/180) \\ A_y &= 0.02 \sin(2\pi \times 50t + 20 \times \pi/180) \\ &\quad + 0.05 \sin(2\pi \times 80t + 20 \times \pi/180) \\ A_z &= 0.03 \sin(2\pi \times 50t + 30 \times \pi/180) \\ &\quad + 0.04 \sin(2\pi \times 80t + 10 \times \pi/180) \\ A_{rx} &= 0.04 \sin(2\pi \times 50t + 40 \times \pi/180) \\ &\quad + 0.03 \sin(2\pi \times 80t + 40 \times \pi/180) \\ A_{ry} &= 0.05 \sin(2\pi \times 50t + 50 \times \pi/180) \\ &\quad + 0.02 \sin(2\pi \times 80t + 50 \times \pi/180) \\ A_{rz} &= 0.06 \sin(2\pi \times 50t + 60 \times \pi/180) \\ &\quad + 0.01 \sin(2\pi \times 80t + 60 \times \pi/180) \end{aligned}$$

where  $t$  is the time variable in units of s;  $A_x$ ,  $A_y$ , and  $A_z$  are the three translational acceleration trajectories in units of  $m/s^2$ , and  $A_{rx}$ ,  $A_{ry}$ , and  $A_{rz}$  are the three angular acceleration trajectories in units of  $rad/s^2$ . When there are no differences between the parameters of the virtual prototype and those of the control model, Table 3 shows the acceleration simulation results obtained at the target frequencies. The maximum errors in the amplitude and phase exceed 6% and 4.49°, respectively, and demonstrate that the simplified dynamic model provides improved accuracy.

To verify the validity of the proposed feedback iterative control method, there is a +5% difference between the parameters of the virtual prototype and those of the control model. The deviations given here can be ensured by careful manufacturing and measurement.

Figure 5 shows the simulation results for  $A_x$  in the time domain under the first iterative control step. The data from the steady-state region are processed using a fast Fourier transform (FFT). Because the micro-vibration excitation is extremely small, the GSP can be approximated as a linear system. Therefore, a sinusoidal excitation input will produce the same frequency output, and the amplitude ratio and the phase deviation will remain relatively stable. Here, the relative phase is used to represent the output stability. The acceleration phases must be converted into relative phases, and the conversion formula required is as follows: Relative Phase  $A_i(\omega_j) = \text{FFT Phase } A_i(\omega_j) - \text{FFT Phase } A_x(\omega_1) + \text{Target Phase } A_x(\omega_1)$  where Relative Phase  $A_i(\omega_j)$  is the relative phase of  $A_i$  at a frequency  $\omega_j$ , FFT Phase  $A_i(\omega_j)$  is the phase of  $A_i$  at the frequency  $\omega_j$  as calculated using the FFT, and Target Phase  $A_x(\omega_1)$  is the desired phase of  $A_x$  at the frequency  $\omega_1$ .

Figures 6 and 7 show the output acceleration amplitudes and phase responses over eight iterations. Table 4 shows a comparison of the acceleration amplitudes, phases, and

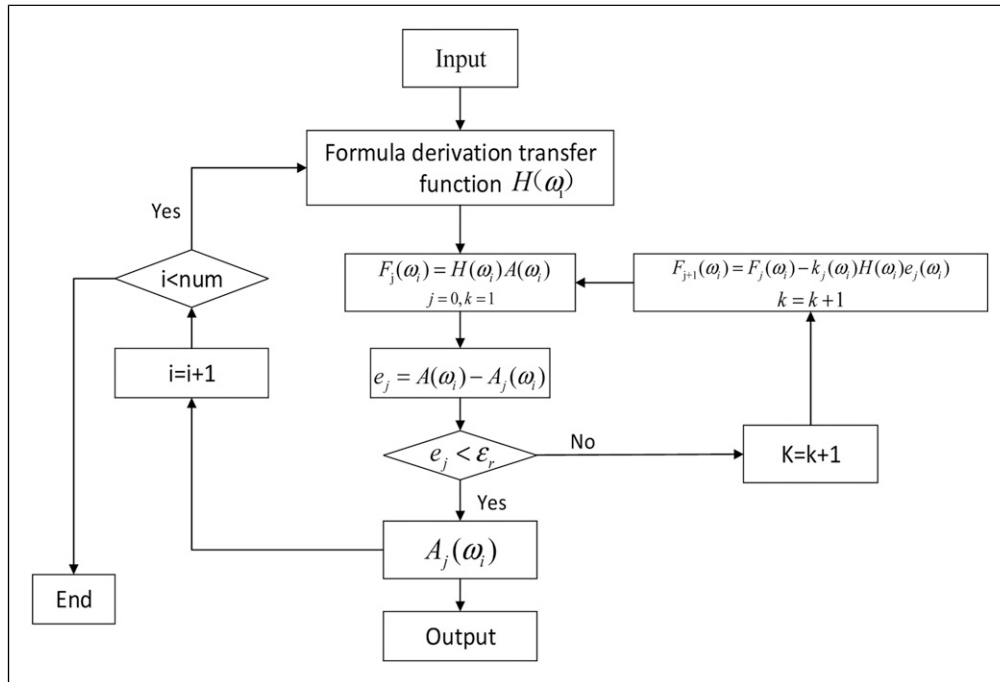


Figure 4. Iterative flowchart for the control process.

Table 1. Structural parameters of the virtual prototype and the control model.

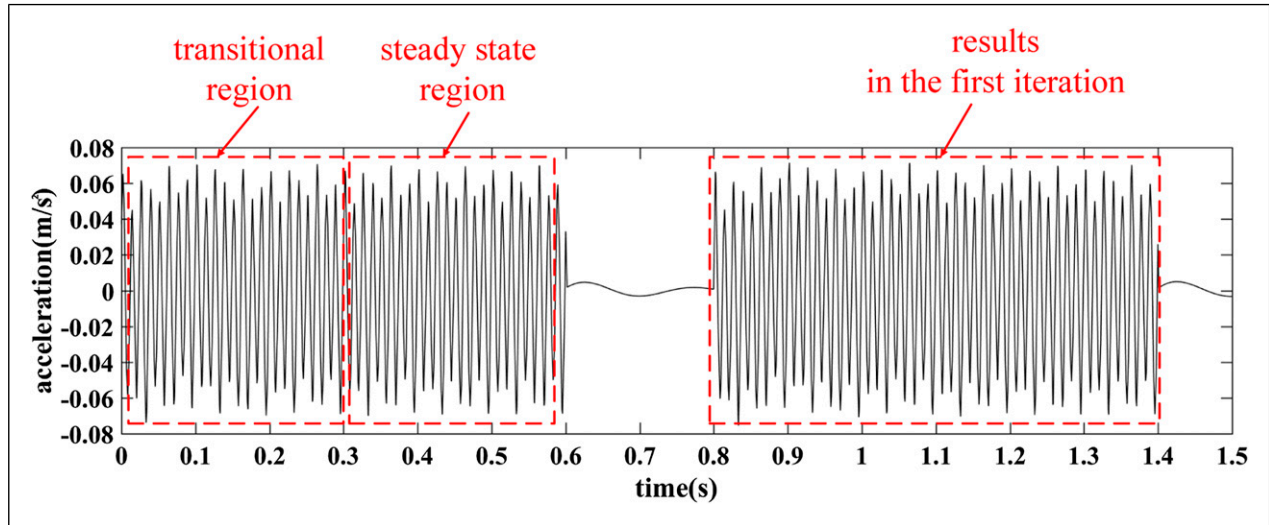
Notation	Statement	Value
$R_p$	Radii of the upper platforms	0.120 m
$R_b$	Radii of the lower platforms	0.18 m
$H$	Height of the origin of the body frame in the base frame	0.22 m
$\varphi$	Upper platform central angle	30°
$\Theta$	Base plane central angle	90°
$r_{rci}$	Distance between the center of upper leg and upper hinge point	81.431 mm
$r_{tci}$	Distance between the center of lower leg and lower hinge point	72.314 mm
$z_{cm}$	Height of the centroid of the moving platform in the body frame	26.789 mm
$K$	Axial stiffness	45221.5 N·m <sup>-1</sup>
$C$	Damping coefficient	300 N/(m/s)

Table 2. Mass properties of the virtual prototype and the control model.

Notation	Statement	Value
$M$	Mass of the upper platform	6.778 kg
$I_{xx}$	Moment of inertia of the rod about the X-axis	4.111 × 10 <sup>-2</sup> kg·m <sup>2</sup>
$I_{yy}$	Moment of inertia of the rod about the X-axis	4.111 × 10 <sup>-2</sup> kg·m <sup>2</sup>
$I_{zz}$	Moment of inertia of the rod about the Y-axis	8.484 × 10 <sup>-2</sup> kg·m <sup>2</sup>
$m_{rci}$	Mass of the rod	0.651 kg
$m_{tci}$	Mass of actuator	2.263 kg
$I_i r$	Principal moment of inertia of the upper leg	2.105 × 10 <sup>-3</sup> kg·m <sup>2</sup>
$I_i t$	Principal moment of inertia of the lower leg	5.593 × 10 <sup>-3</sup> kg·m <sup>2</sup>

**Table 3.** Acceleration simulation results at the target frequencies.

frequency		$A_x$	$A_y$	$A_z$	$A_{rx}$	$A_{ry}$	$A_{rz}$
50 Hz	Amplitude(m/s)	0.0100	0.0198	0.0301	0.0384	0.0488	0.0616
	Phase(°)	10.0000	19.7081	30.2764	40.2434	50.5688	59.8687
80 Hz	Amplitude(m/s)	0.0596	0.0496	0.0401	0.0286	0.0188	0.0102
	Phase(°)	31.9443	21.9167	12.3314	41.1272	54.4888	61.8214



**Figure 5.** Acceleration responses in the time domain under the first iterative control step.

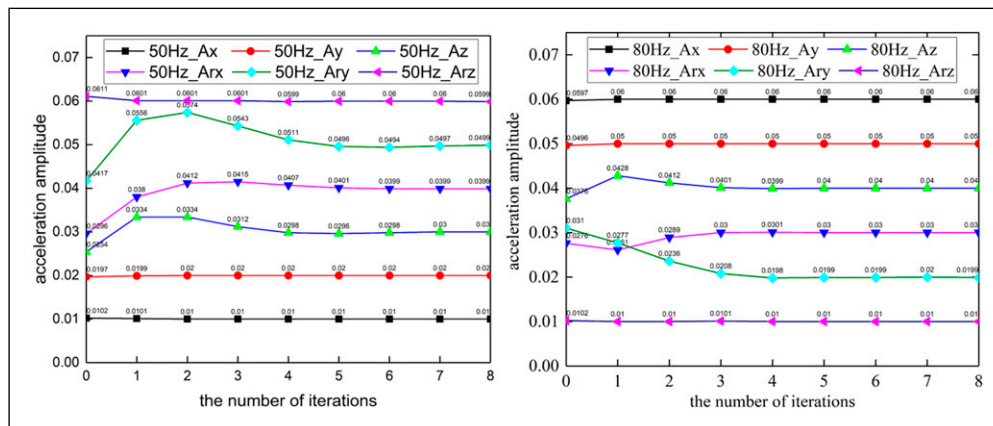


**Figure 6.** Acceleration amplitude responses in the frequency domain during the eight iterations.

errors of the simulation and the eight iterations. The figures and tables clearly show the deviations of the mass and the moment of inertia of the model due to variations in manufacturing and measurement, and the maximum errors in the amplitude and the phase exceed 55% and 60°, respectively; these errors appear in the *Y*-axis angular acceleration at 80 Hz when the initial forces are used to control the platform. After eight iterations, the amplitude errors of

the acceleration and the phase are less than 1% and 0.2°, respectively. This demonstrates that the iterative feedback control method can achieve the required effect.

### 5. Experimental

Micro-vibration experiments were carried out with a 10 kg load to verify the feedback iterative control method. The

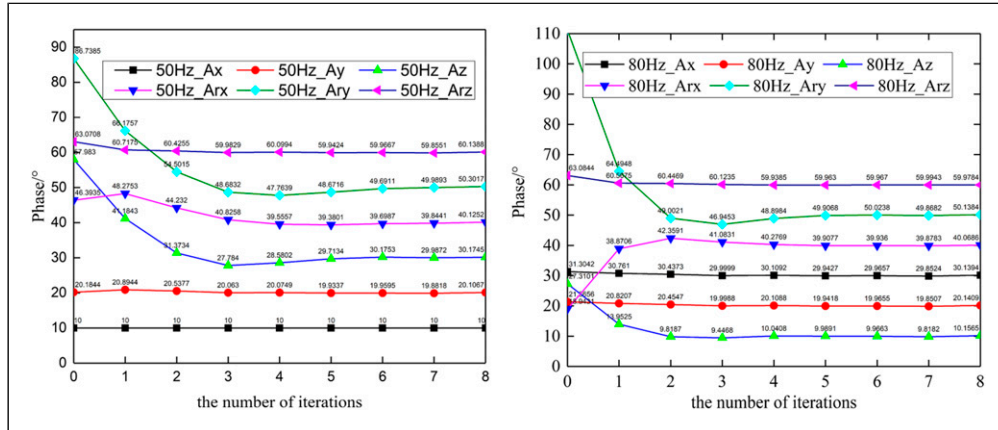


Figure 7. Acceleration phase responses in the frequency domain during the eight iterations.

Table 4. Acceleration iteration results at the target frequencies.

frequency		$A_x$	$A_y$	$A_z$	$A_{rx}$	$A_{ry}$	$A_{rz}$
50 Hz	Target amplitude	0.01	0.02	0.03	0.04	0.05	0.06
	Simulation amplitude	0.0102	0.0197	0.0254	0.0296	0.0417	0.0611
	Relative error	2%	1.5%	15%	26%	16.6%	1.8%
	Iterative amplitude	0.0100	0.0200	0.0300	0.0399	0.0499	0.0599
	Relative error	0	0	0	0.25%	0.2%	0.17%
	Target phase(°)	10	20	30	40	50	60
	Simulation phase(°)	10.0000	20.1844	57.9830	46.3935	86.7385	63.0708
	Relative error	0	0.1844	27.9830	6.3935	36.7385	3.0708
	Iterative phase(°)	10.0000	20.1067	30.1745	40.1252	50.3017	60.1388
Relative error	0	0.1067	0.1745	0.1252	0.3017	0.1388	
80 Hz	Target amplitude	0.06	0.05	0.04	0.03	0.02	0.01
	Simulation amplitude	0.0597	0.0496	0.0376	0.0276	0.0310	0.0102
	Relative error	0.5%	0.8%	6%	8%	55%	2%
	Iterative amplitude	0.0600	0.0500	0.0400	0.0300	0.0200	0.0100
	Relative error	0	0	0	0	0	0
	Target phase(°)	30	20	10	40	50	60
	Simulation phase(°)	31.3042	21.3656	27.3101	18.9431	111.2181	63.0844
	Relative error	1.3042	1.3656	17.3101	21.0569	61.2181	3.0844
	Iterative phase(°)	30.1394	20.1409	10.1565	40.0686	50.1384	59.9784
Relative error	0.1394	0.1409	0.1565	0.0686	0.1384	0.0216	

devices required for the micro-vibration experiments are showed in Figure 8. The circuit board uses a DC power supply to obviate the 50 Hz interference that occurs when using an AC power supply. The six-dimensional attitude is measured through the outputs of the six acceleration sensors installed at six different locations.

The test results (Toyoshima et al., 2010) for the space micro-vibrations show that the micro-vibrations mainly occur within the 100 Hz range; therefore, we set the operating frequency to be within 100 Hz in these experimental tests. Single frequency and multifrequency micro-vibration tests were conducted and the desired accelerations, iterative accelerations, and relative errors are presented in Table 5.

The control model’s damping coefficient is set to zero in these micro-vibration tests.

Figures 9 and 10 show the acceleration response curves obtained in the frequency domain in the micro-vibration tests. It can be seen from the figures and table that the maximum amplitude error of single frequency experiment is 6.67% appearing in X-axis angular acceleration and the maximum phase error is 8.79% appearing in Z-axis angular acceleration; the maximum amplitude error of multifrequency experiment is 7.5% appearing in X-axis angular acceleration at 40 Hz, the maximum phase error is 8.79° appearing in Z-axis angular acceleration, 7.5° in X-axis angular acceleration at 40 Hz, and 14.26° at 60 Hz.

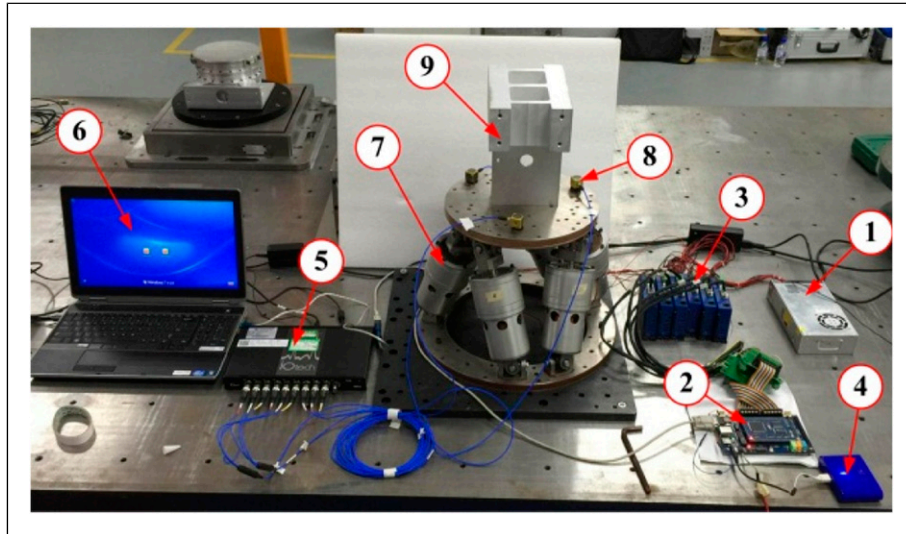


**Figure 8.** Micro-vibration experiments with the 10 kg load. (1) A power supply for the power amplifier, (2) a circuit board, (3) a power amplifier, (4) a power supply for the circuit board, (5) a spectrum analyzer, (6) a data acquisition computer, (7) a micro-vibration parallel manipulator, (8) an acceleration sensor, and (9) the 10 kg load.

**Table 5.** Desired accelerations for the micro-vibration tests.

frequency			$A_x$	$A_y$	$A_z$	$A_{rx}$	$A_{ry}$	$A_{rz}$
Trial 1	60 Hz	Target amplitude	0.01	0.02	0.03	0.03	0.02	0.01
		Iterative amplitude	0.0102	0.0199	0.0298	0.0300	0.0203	0.0101
		Relative error	2%	0.5%	0.67%	0	1.5%	1%
	40 Hz	Target phase(°)	0	0	0	0	0	0
		Iterative phase(°)	0	0.14	0.26	-0.17	0.58	0.33
		Relative error(°)	0	0.14	0.26	0.17	0.58	0.33
		Target amplitude	0.02	0.02	0.02	0.02	0.02	0.02
		Iterative amplitude	0.0202	0.0201	0.0201	0.0200	0.0200	0.0200
		Relative error	2%	0.5%	0.5%	0	0	0
		Target phase(°)	0	10	30	45	20	10
Trial 2	60 Hz	Iterative phase(°)	0	9.71	30.45	44.56	20.87	10.88
		Relative error(°)	0	0.29	0.45	0.44	0.87	0.88
		Target amplitude	0.03	0.03	0.03	0.03	0.03	0.03
		Iterative amplitude	0.0299	0.0300	0.0299	0.0302	0.0303	0.0298
		Relative error	0.33%	0	0.33%	0.67%	1%	0.67%
	100 Hz	Target phase(°)	10	20	30	45	50	60
		Iterative phase(°)	10.41	20.22	30.57	45.73	50.45	59.68
		Relative error(°)	0.41	0.22	0.57	0.73	0.45	0.34
		Target amplitude	0.05	0.05	0.03	0.02	0.03	0.04
		Iterative amplitude	0.05	0.0498	0.0299	0.0197	0.0300	0.0400
		Relative error	0	0.4%	0.33%	1.5%	0	0
		Target phase(°)	45	45	45	45	45	45
		Iterative phase(°)	45.38	44.65	45.77	44.13	44.28	45.79
		Relative error(°)	0.38	0.35	0.77	0.87	0.72	0.79

The errors are controlled by 1–2 iterations; however, to get closer to the real micro-vibration, three iterations of acceleration in six directions are carried out; the amplitude error for the output accelerations relative to the target

accelerations is less than 3% and the phase error for the output accelerations relative to the target accelerations is less than 1°. These results indicate that the control strategy provides high precision for micro-vibration

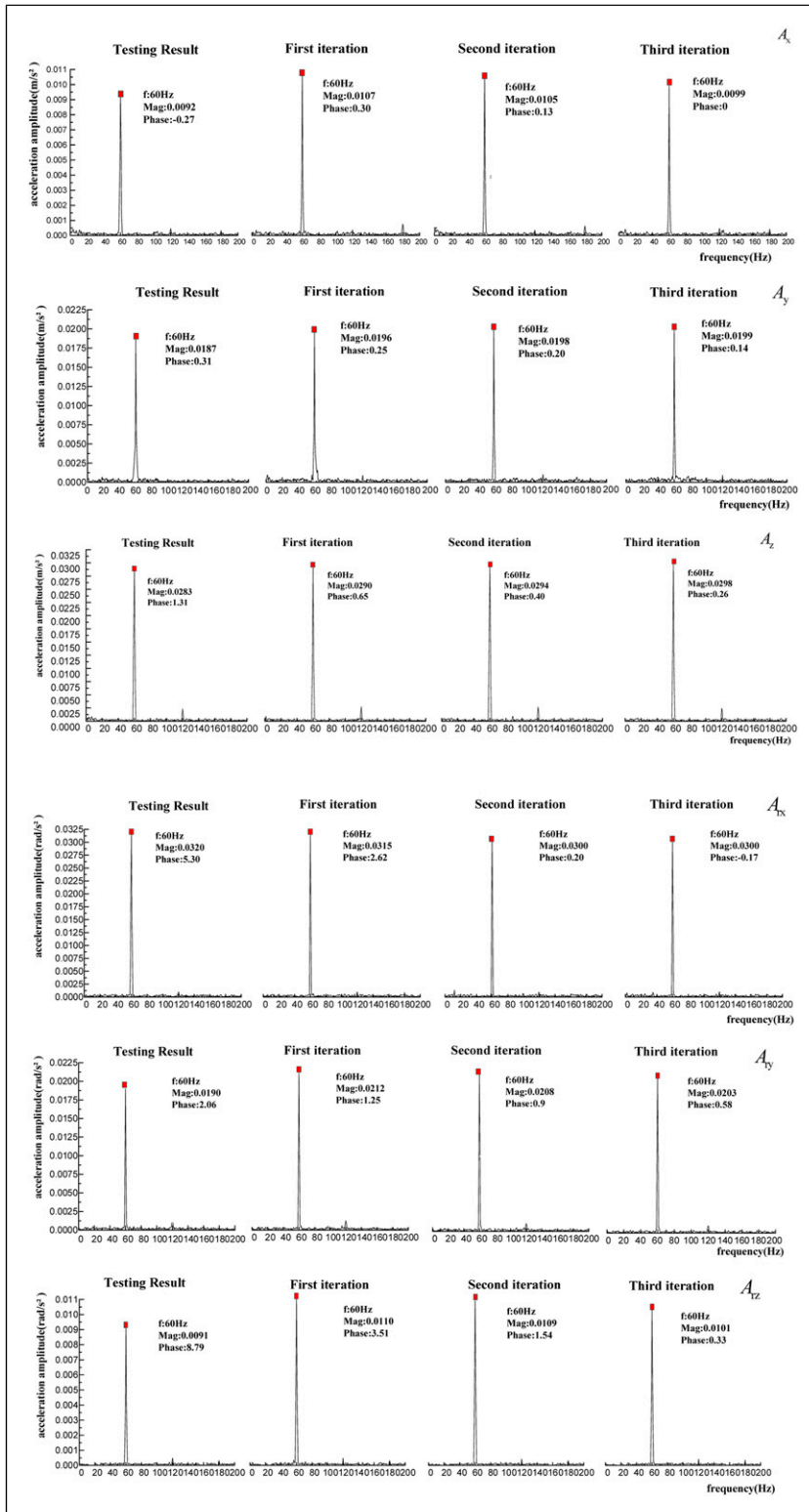


Figure 9. Acceleration response curves obtained in the frequency domain from the single frequency micro-vibration tests.

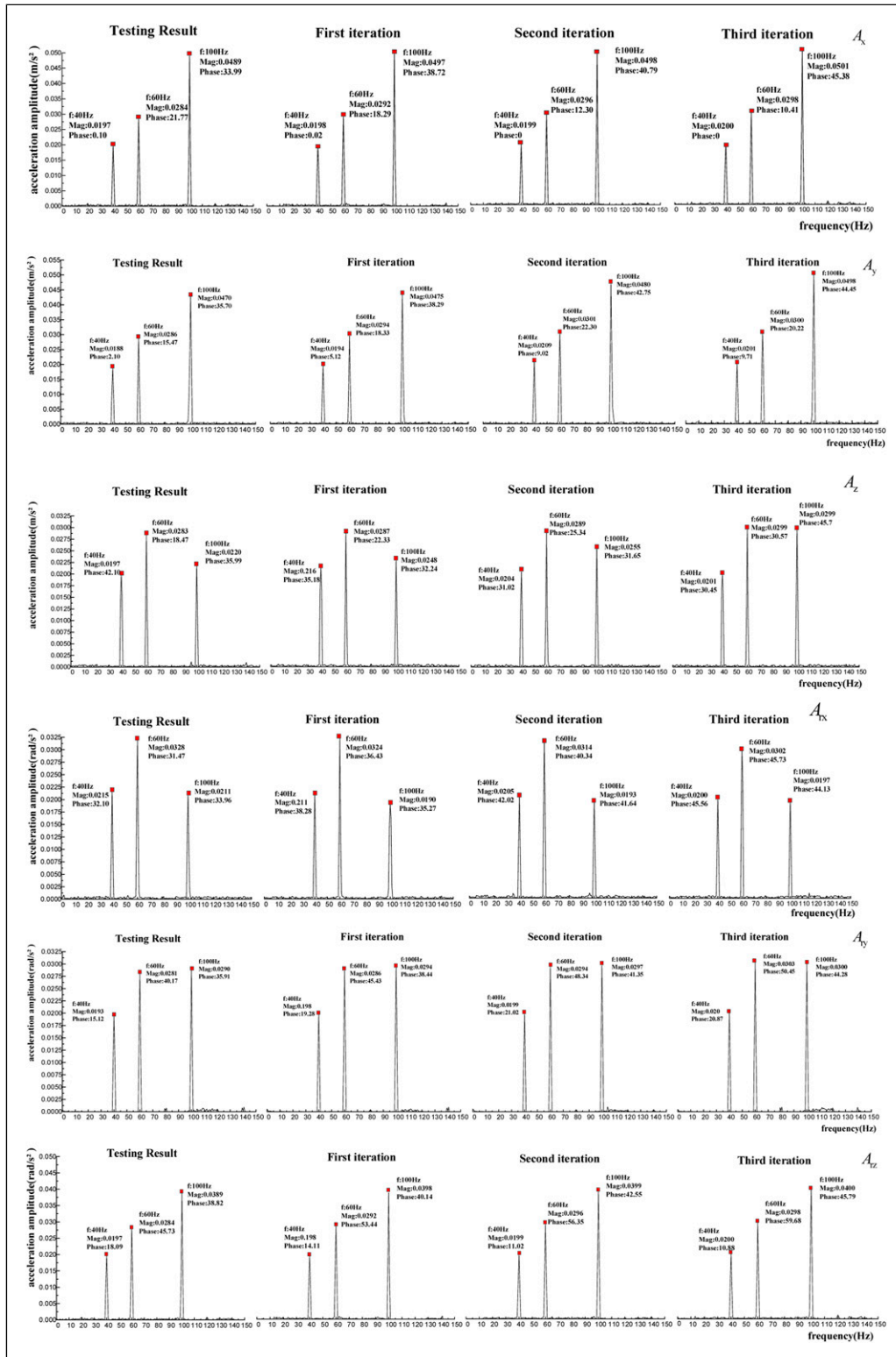


Figure 10. Acceleration response curves obtained in the frequency domain from the multifrequency micro-vibration tests.

control and can thus be used for micro-vibration control in practice.

## 6. Conclusion

A 6-MVP that can reproduce the 6-DOF micro-vibrations at the installation surface for space-based sensitive instruments is introduced in this article. Considering that micro-vibrations have characteristics that include low vibration frequencies, small displacements, and complex forms, the dynamic model is simplified and a feedback iterative control method based on the frequency response model is proposed to control the 6-MVP. Using ADAMS and MATLAB/Simulink, co-simulations were performed to verify the validity of the simplified dynamic model and the associated control method. The results obtained from the micro-vibration experiments show that after several iterations, the amplitude control error is less than 3% and the phase control error is less than 1°. The control strategy presented in this article has the advantages of a simple algorithm and high precision and can also be used to control other similar micro-vibration platforms.

## Acknowledgements

We thank David MacDonald, MSc, from Liwen Bianji, Edanz Editing China ([www.liwenbianji.cn/ac](http://www.liwenbianji.cn/ac)), for editing the English text of a draft of this manuscript.

## Declaration of conflicting interests

The author(s) declared no potential conflicts of interest with respect to the research, authorship, and/or publication of this article.

## Funding

The author(s) disclosed receipt of the following financial support for the research, authorship, and/or publication of this article: This work was supported by the National Natural Science Foundation of China (grant numbers 11672290 and 51705083); the Jilin Scientific and Technological Development Program (grant number 20200404204YY).

## ORCID iD

He Zhu  <https://orcid.org/0000-0002-6539-9601>

## References

- Dasgupta B and Mruthyunjaya TS (1998) A Newton-Euler formulation for the inverse dynamics of the Stewart platform manipulator. *Mechanism and Machine Theory* 33(8): 1135–1152.
- Guo H, Liu Y, Liu G, et al. (2008) Cascade control of a hydraulically driven 6-DOF parallel robot manipulator based on a sliding mode. *Control Engineering Practice* 16(9): 1055–1068.
- Kamesh D, Pandiyan R and Ghosal A (2012) Passive vibration isolation of reaction wheel disturbances using a low frequency flexible space platform. *Journal of Sound and Vibration* 331(6): 1310–1330.
- Kim HS, Cho YM and Lee K-II (2005) Robust nonlinear task space control for 6 DOF parallel manipulator. *Automatica* 41(9): 1591–1600.
- Liu KC, Maghami P and Blaurock C (2012) Reaction wheel disturbance modeling, jitter analysis, and validation tests for solar dynamics observatory. In: AIAA guidance, navigation and control conference and exhibit. Honolulu, Hawaii, 18–21 August 2008. AIAA. DOI: [10.2514/6.2008-7232](https://doi.org/10.2514/6.2008-7232)
- Lin N (2019) Structural Design and Simulation Experimental Study of Six Dimensional Disturbance Simulator. *Journal of Mechanical Strength* 42(01): 140–145.
- Oftadeh R, Aref MM and Taghirad HD (2010) Explicit dynamics formulation of Stewart-Gough platform: a Newton-Euler approach. In: Proceedings 2010 IEEE international conference on intelligent robots and systems, Taipei, Taiwan, 18–22 October 2010. IEEE. DOI: [10.1109/IROS.2010.5653157](https://doi.org/10.1109/IROS.2010.5653157)
- Park G, Lee DO, Han JH, et al. (2012) Development of multi-DOF active microvibration emulator. In: ASME conference on smart materials. Georgia, USA, 19–21 September 2012. ASME. DOI: [10.1115/SMASIS2012-8240](https://doi.org/10.1115/SMASIS2012-8240)
- Park G, Lee DO and Han JH (2014) Development of multi-degree-of-freedom microvibration emulator for efficient jitter test of spacecraft. *Journal of Intelligent Material Systems and Structures* 25(9): 1069–1081.
- Pedrammehr S, Mahboubkhah M and Khani N (2012) Improved dynamic equations for the generally configured Stewart platform manipulator. *Journal of Mechanical Science and Technology* 26(3): 711–721.
- Toyoshima M, Takayama Y and Kunimori H (2010) In-orbit measurements of spacecraft microvibrations for satellite laser communication links. *Optical Engineering* 49(8): 498–578.
- Vose TH, Turpin MH, Dames PM, et al. (2013) Modeling, design, and control of 6-DoF flexure-based parallel mechanisms for vibratory manipulation. *Mechanism and Machine Theory* 64(6): 111–130.
- Wang X, Xu Z, He S, et al. (2017) Modeling and analysis of a multi-degree-of-freedom micro-vibration simulator. *Shock and Vibration* 2017: 1–17.
- Wang X, Xu Z, Xia M and et al. (2018) Research on a six-degree-of-freedom disturbance force and moment simulator for space micro-vibration experiments. *Journal of Sound and Vibration* 432: 530–548.
- Yang C, He J, Han J, et al. (2009) Real-time state estimation for spatial six-degree-of-freedom linearly actuated parallel robots. *Mechatronics* 19(6): 1026–1033.
- Yang J, Xu Z, Wu Q, et al. (2016) Dynamic modeling and control of a 6-DOF micro-vibration simulator. *Mechanism and Machine Theory* 104: 350–369.
- Zhou W, Liu D, Luo Q, et al. (2012) Analysis and testing of microvibrations produced by momentum wheel assemblies. *Chinese Journal of Aeronautics* 25(4): 640–649.
- Zhou W and Liu D (2013) Experimental research on a vibration isolation platform for momentum wheel assembly. *Journal of Sound and Vibration* 332(5): 1157–1171.